



Calotropis gigantea Fiber-Based Sensitivity-Tunable Strain Sensors with Insensitive Response to Wearable Microclimate Changes

Junze Zhang^{1,2} · Jing Liu^{1,2} · Zeyu Zhao^{1,2} · Weiwei Sun^{1,2} · Gaojuan Zhao³ · Jingge Liu^{1,2} · Jianchu Xu³ · Yuling Li⁴ · Zekun Liu^{5,6} · Yi Li⁵ · Gang Li^{1,2}

Received: 4 November 2022 / Accepted: 3 February 2023 / Published online: 17 March 2023
© Crown 2023

Abstract

Wearable tensile strain sensors have attracted substantial research interest due to their great potential in applications for the real-time detection of human motion and health through the construction of body-sensing networks. Conventional devices, however, are constantly demonstrated in non-real world scenarios, where changes in body temperature and humidity are ignored, which results in questionable sensing accuracy and reliability in practical applications. In this work, a fabric-like strain sensor is developed by fabricating graphene-modified *Calotropis gigantea* yarn and elastic yarn (i.e. Spandex) into an independently crossed structure, enabling the sensor with tunable sensitivity by directly altering the sensor width. The sensor possesses excellent breathability, allowing water vapor generated by body skin to be discharged into the environment (the water evaporation rate is approximately $2.03 \text{ kg m}^{-2} \text{ h}^{-1}$) and creating a pleasing microenvironment between the sensor and the skin by avoiding the hindering of perspiration release. More importantly, the sensor is shown to have a sensing stability towards changes in temperature and humidity, implementing sensing reliability against complex and changeable wearable microclimate. By wearing the sensor at various locations of the human body, a full-range body area sensing network for monitoring various body movements and vital signs, such as speaking, coughing, breathing and walking, is successfully demonstrated. It provides a new route for achieving wearing-comfortable, high-performance and sensing-reliable strain sensors.

Keywords Wearable strain sensor · Functionalized *Calotropis gigantea* fiber · Wearable microclimate · Graphene coating · Tunable sensitivity

Introduction

Real-time body area detection by flexible on-skin strain sensors has attracted tremendous attention owing to their exciting potential in personal healthcare management,

motion monitoring and human–machine communication [1–12]. Typical electrical strain sensors implement the function by converting the physical deformations of the human body into electrical signals. Much research has been carried out on strain sensors predominantly focuses on enhancing the sensitivity, sensing range, and reliability of strain sensors by encapsulating conductive networks

Junze Zhang and Jing Liu contributed equally.

✉ Zekun Liu
zekun.liu@ndorms.ox.ac.uk

✉ Yi Li
henry.yili@manchester.ac.uk

✉ Gang Li
tcligang@suda.edu.cn

¹ National Engineering Laboratory for Modern Silk, College of Textile and Clothing Engineering, Soochow University, Suzhou 215123, China

² Jiangsu Advanced Textile Engineering Technology Center, Nantong 226007, China

³ Honghe Center for Mountain Futures, Kunming Institute of Botany, Chinese Academy of Sciences, Honghe County, Yunnan 654412, China

⁴ Key Laboratory of Textile Science and Technology, Ministry of Education, Donghua University, Shanghai 201620, China

⁵ Department of Materials, University of Manchester, Oxford Road, Manchester M13 9PL, UK

⁶ Botnar Research Center, University of Oxford, Old Road, Headington OX3 7LD, Oxford, UK

with elastomers [13, 14] rather than improving the wearing performance, such as physical comfort, which is greatly related to the sensor's permeability. Thus, the permeability to air and moisture that is essential, especially in regard to long-term use, is frequently neglected. The human body's process of involuntary breathing continuously generates sweat, which evaporates in the form of moisture, and the intensity of the sweat generated, increases during exercise. A sensor without or with low permeability certainly causes wearing discomfort and even skin irritation [15–19]. It is highly desirable to develop a wearable strain sensor with high breathability to excrete diverse metabolites, thus creating a comfortable microenvironment between the sensors and the skin.

Implementing the sensing function of wearable sensors requires attaching the device to the skin surface [20–25]. Although most sensors can sense physical deformation in a stable environment, the human skin is a complicated physiological system that continuously releases heat to the exterior environment and constantly generates sweat [26, 27]. These metabolites produced by the human body change the temperature and humidity of the microenvironment. Thus, deteriorative sensing reliability and accuracy are the result of using a sensing device that is unable to adjust to the abovementioned environmental stimulations [28, 29]. It is of vital importance to develop a breathable and sensing-reliable sensor that can freely excrete skin metabolites into the surrounding environment to create a comfortable microenvironment and maintain sensing stability and accuracy against wearable microclimate changes.

Calotropis gigantea fiber (CGF) has attracted wide attention in recent years due to its excellent warmth retention and outstanding antibacterial properties [30, 31]. CGF possesses 80–90% hollow structure, which is also a new and unique fiber, exhibiting outstanding hydrophilic or oleophilic properties. Compared to other natural fibers, such as wool, cotton, linen fibers, the CGF has fewer natural curls in the longitudinal direction, leading to a smoother and softer surface [32]. The CGF has the potential to be used in the development of wearable electronic devices due to the abovementioned advantages. Graphene has been frequently applied to prepared conductive fibers, as it possesses high electrical conductivity, great mechanical strength, and superior chemical stability [33, 34]. Moreover, it can easily cover the fiber surface under shearing force and form interconnected electron-transport pathways for high electrical conductivity owing to the strong π – π interactions existing between adjacent graphene. However, few studies have reported on strain sensors using the combination of CGF and graphene.

Herein, a highly breathable graphene-modified fabric (GMF) strain sensor with an insensitive response to changes

in temperature and humidity within a certain range was developed. It is artistically fabricated into a crisscross structure consisting of graphene-modified conductive *Calotropis gigantea* yarn (CGY) and elastic yarns. The sensor shows a fast response speed (less than 60 ms) and excellent durability (10% strain for 3000 cycles), and its sensitivity can be altered by simply altering the width of the fabric. Owing to the high-porosity of the fabric structure, the GMF sensor exhibits excellent breathability to air and water vapor ($2.03 \text{ kg m}^{-2} \text{ h}^{-1}$). Remarkably, taking advantage of the high hydrophobicity and insensitivity to temperature changes of reduced graphene oxide (rGO) after a long reduction time, the GMF sensor possesses sensing independence against temperature and relative humidity ranges from 22.8 to 47.3 °C and 39–71%, respectively. The sensor is demonstrated that it can monitor human motions and vital signs such as speaking, chewing, coughing, breathing, joint bending and sports in full-range body-sensing networks. Thus, a new route for developing a functional sensor with tunable sensitivity, high breathability and sensing reliability is proposed.

Experimental Section

Materials

Natural graphite was purchased from Suzhou Industrial Park Bomeida Reagent Instrument Co., Ltd. The CGYs and elastic yarns were provided by Yixing Zhongchang Yarn-dyed Co., Ltd. and Haining Xianya Coveredspandexyarn Co., Ltd. Silver paste and copper wires were obtained from Shenzhen Xinwei Electronic Materials Co., Ltd. and Luoyang Zhanyuan Copper Co., Ltd. Analytical-grade sodium, hydrochloric acid, and potassium permanganate reagents were purchased from Sinopharm Chemical Reagent Co., Ltd, China. Concentrated sulfuric acid, hydrogen peroxide at a concentration of 30%, and ascorbic acid were supplied by Jiangsu Qiangsheng Functional Chemical Co., Ltd, China, Shanghai Lingfeng Chemical Reagent Co., Ltd, China, and Suzhou Ketong Biomedical Technology Co., Ltd, China, respectively.

Fabrication Process of the GMF Sensors

The pristine CGY was immersed in the GO solution (synthesized by the Hummers method [35]) for 2 h before coating, and then the CGY was padded by a miniature rolling mill to remove the excess GO from the surface. After that, the coated yarns were placed in an oven at 60 °C for 24 h. Using the green reducing agent ascorbic acid to reduce the GO-modified CGY (GO-CGY) at 80 °C for 24 h, the

rGO-modified CGY (rGO-CGY) was prepared. The elastic yarns and a conductive CGY were arranged in the longitudinal direction and crosswise direction, where they were individually staggered using automatic weaving equipment to form a GMF with a conductive sensing network. The GMF sensors were prepared by cutting the GMF into rectangular ($4 \times 2 \text{ cm}^2$) pieces. Conductive silver paste and copper wires were attached to both ends of the rectangular pieces.

Characterization

The surface morphologies and elemental distribution of the CGYs and the GMFs were measured using a scanning electron microscope (SEM, Hitachi TM3030, Tokyo, Japan). The surface roughness of the CGYs was measured using atomic force microscopy (AFM, Dimension Loon, Bruker Company, USA). The surface hydrophilicity of the GMFs was measured with contact angle measuring equipment (Krüss DSA 100, Germany). The tensile properties of the CGYs were tested by a universal material testing machine (INSTRON-3365, Instron, USA). A Raman spectroscopy (Jobin Yvon LabRam HR800) with a 632.8 nm laser wavelength and Fourier transform infrared spectroscopy (FT-IR) (Nicolet 5700, USA) were used to measure the structure of the CGYs. The resistance of the rGO-CGY was measured with a Keithley DMM7510 instrument. Targeted strain was applied to the sensor using a linear motor module, and all electrical signals generated from the sensors were collected by a multimeter (Keithley DMM7510).

Results and Discussion

Figure 1a exhibits the procedure of functionalizing the CGY by pad dyeing. The pristine CGY was immersed in the GO solution and passed through a miniature rolling mill to achieve the GO dyeing. Then, the GO-modified CGYs were dried in an oven at 60°C for 24 h. The green reducing agent ascorbic acid was chosen to reduce the GO on the surface of the pristine CGY at 80°C for 24 h. Fig. S1 (b₁–b₄) illustrate the surface morphology of the pristine CGY and the rGO-CGY. The pristine CGY possesses a smooth surface, which is consistent with the previous literature [36]. In contrast, the functionalized CGY displays a coarse and uneven surface that is similar to graphene fibers [37, 38]. The volume shrinkage is beneficial for graphene to obtain a compact structure on the fibers' surface, forming an efficient electron transmission path and obtaining high conductivity [39].

By taking advantage of the flexible patterns of woven structures, the GMF sensor is fabricated into plain and twill structures using automatic weaving equipment (Fig. S1a–d). Figure 1c presents schematic diagrams of the GMF, where the prepared GMF, which has an independent crossed

structure, maintains good flexibility, allowing it to be freely bent to a high degree. The GMF consists of rGO-CGY and elastic spandex (Fig. 1d) with an interlaced structure, the surface morphology of which is shown in Fig. S1e–g. The excellent elasticity of the elastic yarns endows the GMF with high stretchability upon deformation parallel to the elastic yarns (Fig. 1e1–e2). As a proof-of-concept illustration of the breathability of the GMF sensor, Fig. 1f displays a schematic diagram of the skin-wearable sensor-environment system. It reveals that body metabolites from skin can freely discharge to air in the form of water vapor when the sensor is worn due to the porous structure of the GMF.

Figure 2a exhibits the electrical performance of the rGO-CGY with a length of 5 cm and indicates that the electrical conductivity of the rGO-CGY increases with increasing coating times. The resistance of the CGY is about 2500 k Ω after pad dyeing 1 time. While the electrical resistance becomes approximately 503 k Ω after coating 7 times. Then, the electrical resistance declines slowly to approximately 300 k Ω after 10 treatments and only reaches about 221 k Ω after 15 coating treatments are applied. Considering the complexity and efficiency of the process, more pad dyeing times will increase the damage to the CGY. The rGO-CGYs treated 7 times and 10 times were selected to compare the relationship between the number of graphene coating applications and yarn performance after functionalization, which are defined as the rGO-CGY-7 and the rGO-CGY-10, respectively. Figure 2b shows that the electrical conductivities of rGO-CGY-7 and rGO-CGY-10 are 3.5 S/m and 6.5 S/m, respectively. With more pad dyeing cycles, the rGO-CGY contains more electron-transport pathways and obtains higher electrical conductivity because the strong π – π interactions between adjacent graphene form interconnected electron-transport pathways after reduction [40, 41]. The mechanical curves of the CGYs in Fig. 2c reveal that the graphene coating can result in a higher breaking strength and a lower elongation. The breaking strength of the pristine CGY is approximately 166 cN, and it increases to approximately 203 cN after a graphene coating is applied 10 times (Fig. S2a). The attachment of graphene, which possesses high mechanical strength, on the fiber surface promotes a stronger combination between fibers. The negatively charged GO species and positively charged hydrogen in the CGY are bonded by electrostatic attraction, which also endows the CGY with higher breaking strength [42, 43]. The tensile strain of the CGYs decreases slightly as the number of pad dyeing cycles increases, with tensile strains of 7.2% and 4.5% for the pristine CGY and the rGO-CGY-10, respectively (Fig. S2b).

The Raman spectra in Fig. 2d reveal that there are two distinct characteristic peaks for the CGY functionalized by the GO and the rGO, which represent the D-band at 1370 cm^{-1} (related to defects or heteroatom-doping) and

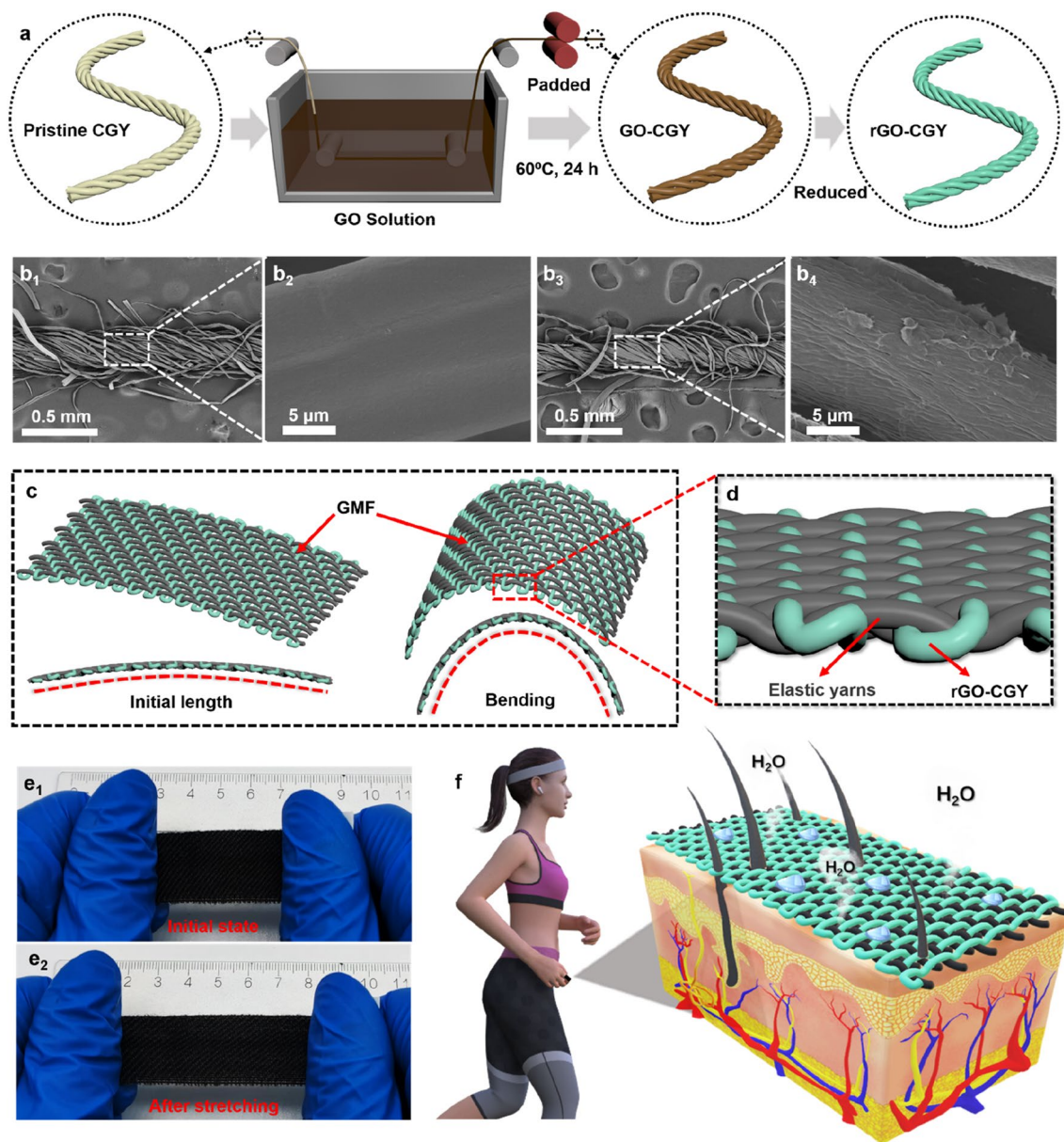


Fig. 1 Illustration of the GMF fabrication process. **a** Schematic diagram of the preparation of rGO-CGY. **b**₁, **b**₂ the pristine CGY and **b**₃, **b**₄ the rGO-CGY. **c**, **d** Structure illustrations of the GMF with a twill structure. **e**₁–**e**₂ Photographs of the

GMF under initial and stretched conditions. **f** Schematic diagram of the skin-wearable sensor-environment system, which demonstrates the breathability of the sensor

the G-band at 1590 cm^{-1} (attributed to the vibrations of the sp^2 -bonded crystalline carbon). It indicates the existence of a carbonaceous structure on the CGY surface [44]. By fitting the curves (Fig. S3a–b), it exhibits that the intensity ratio of the D-band and the G-band increases from 0.6 to 1.3, while the full width at half maximum of the D-band decreases from 123 to 95 (Fig. S3c). The enhancement of the D-band is mainly attributed to the formation of small-sized sp^2 domains (disordered carbon) during the reduction process. The decrease in the full width at half maximum

suggests an increase in the structural order. These changes reveal that the GO is chemically converted into the rGO, which is consistent with the findings reported in the literature [44]. The FT-IR spectra shown in Fig. 2e indicate characteristic peaks of graphene at approximately 3340 cm^{-1} , 2905 cm^{-1} , 1638 cm^{-1} , 1430 cm^{-1} and 1060 cm^{-1} for the OH stretching, asymmetrical C–H stretching, C=O stretching, CH_2 symmetrical bending and C–O stretching, respectively [45]. The peak at 1638 cm^{-1} disappears, and the peaks at 2905 cm^{-1} and 3340 cm^{-1} become weaker, implying that

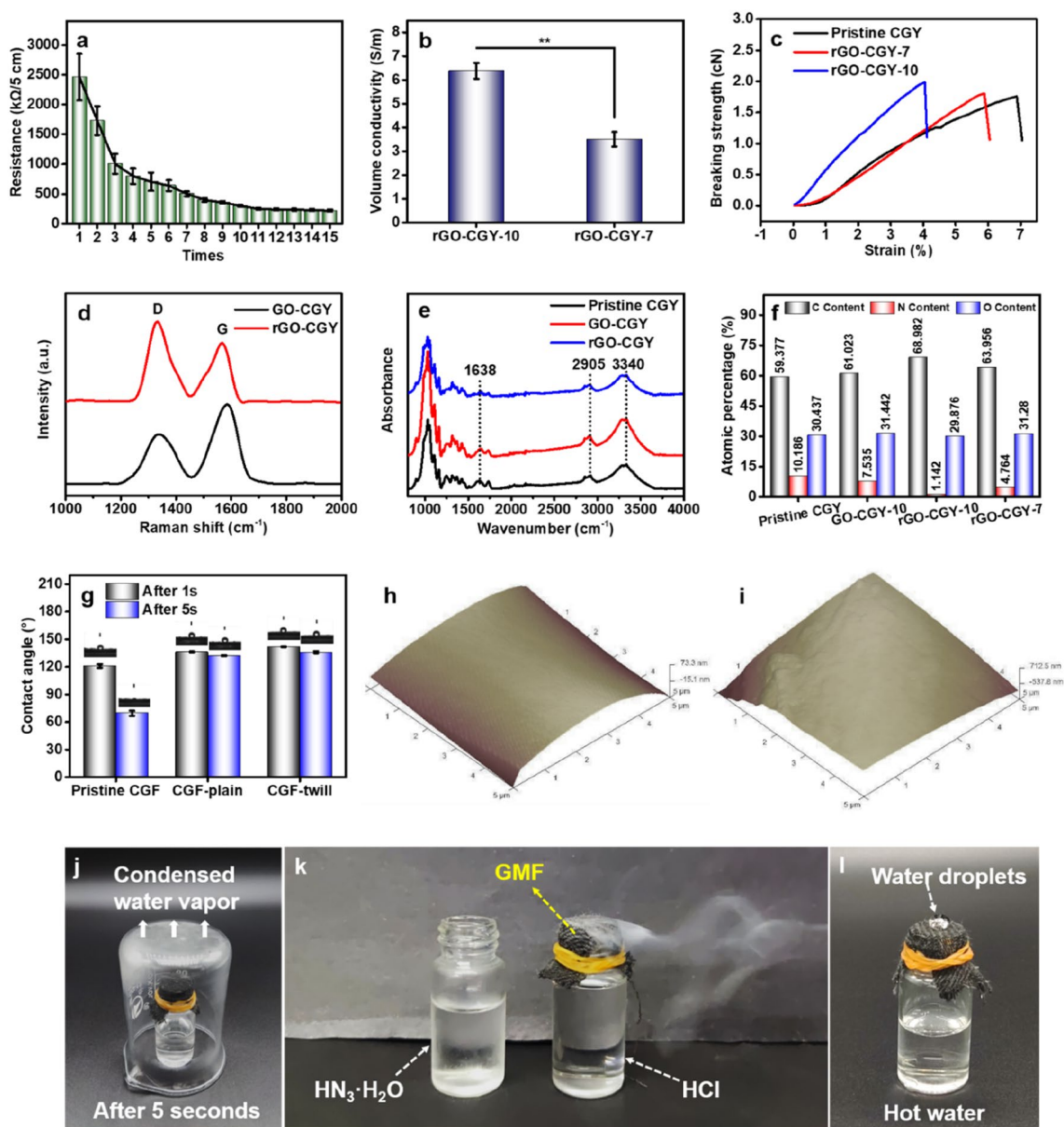


Fig. 2 Characterization of the rGO-CGYs and the functionalized GMF. **a** Electrical resistance changes of the rGO-CGY with increasing pad dyeing times. **b** Volume electrical conductivity of the rGO-CGY-10 and the rGO-CGY-7. **c** Mechanical curves of the CGYs. **d** Raman spectroscopy of functionalized CGYs. **e** FT-IR spectra of the pristine CGY, the GO-modified CGY, and the rGO-CGY. **f** Surface element content of the CGYs. **g** Contact angle of the CGYs before

and after functionalization. AFM images of **h** the pristine CGY and **i** the rGO-CGY. **j** Photograph showing the water vapor transmission performance of the GMF. **k** Photograph of hydrogen chloride gas escaping from the vial covered with the GMF. **l** Photograph of a water droplet on the surface of the GMF to display that it is water-proof when exposed to water vapor

the GO on the surface of the CGY is successfully reduced to the rGO after the treatment. The process of functionalization significantly changes the surface elements, of which the atomic percentages of C, N, and O are 59.377%, 10.186%, and 30.437%, respectively, for the pristine CGY, while they become 61.023%, 7.535%, and 31.442% after GO modification (Fig. 2f). C increases to 68.982%, N and O decrease to 1.142% and 29.876% after reduction, which indicates that

the reduction process successfully facilitates the transformation of the rGO from the GO. Compared to the rGO-CGY-10, the C on the surface of the rGO-CGY-7 occupies a lower proportion (63.956%), and the O and N increase to 4.764% and 31.28%, respectively. The difference can be attributed to more graphene covering the surface of the CGY with increasing pad dyeing times [46]. The element conversion is also characterized by observing their distribution,

which shows that the corresponding elements are evenly distributed throughout without agglomeration (Fig. S4).

To assess the wash fastness of the CGYs, the rGO-CGY was washed with deionized water and laundry liquid for 60 min (see the details in Fig. S5). The electrical conductivity of the functionalized yarn decreases slightly from approximately 6.5–5.6 S/m. The minor deterioration is mainly due to the abrasion of the graphene layer on the fiber surface during the washing process. The functionalized CGY continues to maintain good electrical conductivity after washing in both deionized water and laundry liquid, which indicates that the rGO-CGY has good wash fastness due to the strong binding force between the graphene and fiber. Figure 2g shows the changes in the water contact angles of the GMFs with changes in the dipping time. The contact angle of the pristine GMF (both the longitudinal and crosswise yarns are the pristine CGYs) is about 121° (dipping time is 1 s), and the contact angle decreases to approximately 69° after 5 s due to the abundant hydrophilic functional groups on the CGY surface. In contrast, the GMFs with different structures acquire higher contact angles during this process, reaching approximately 136° and 142° for the plain and twill fabrics, respectively (dipping time is 1 s). They maintain high contact angles (132° and 135°) after 5 s, which is due to the hydrophobicity of the rGO [47]. After reduction treatment, some of the oxygen-related functional groups on the fiber surface are eliminated [48]. On the other hand, graphene coating also increases the surface roughness of the CGY, resulting in high hydrophobicity [49]. The surface roughness values of the pristine CGY and the rGO-CGY from the GMFs, which are 73.3 nm and 712.5 nm, respectively, can be observed in the AFM images (Fig. 2h–i). Compared to the pristine CGYs with smooth surfaces, the rGO-CGYs exhibit rough and uneven surfaces due to the existence of graphene layers that have wrinkled and crumpled surfaces [50] (Figs. S6a–f).

To demonstrate the excellent breathability of the GMF, we bound it to the opening of a vial placed in a beaker by a rubber band (Fig. 2j). The figure shows that the water vapor can pass through the fabric and escape from the vial containing hot water (> 80 °C), which reveals its water vapor permeability. Similarly, hydrochloric acid can freely pass through the breathable fabric, which is demonstrated by covering the top of a vial with hydrochloric acid inside with fabric and then allowing it to react with ammonia (Fig. 2k). The white ammonium chloride smoke from the chemical reaction can be observed above the fabric, indicating that the GMF does not restrict or block the diffusion of hydrochloric acid gas from the vial to the environment. To quantitatively evaluate the breathability of the fabric, the mass change of the water in the vial with the GMF covering the opening at 50 °C is recorded. Fig. S7 illustrates the typical

curves of the time-dependent mass change of the water. The evaporation rate calculated from the curves indicates that the water evaporation rate is 2.03 kg m⁻² h⁻¹ for the GMF, and it maintains a similar level after the fabric undergoes 100 cycles of stretching under a strain of 15%. A water droplet is applied to the surface of the GMF (Fig. 2l), and the droplet remains its initial state without being absorbed by the GMF in an environment where water vapor from the hot water is present. This shows that the good waterproofness of the GMF can effectively prevent metabolites such as liquid sweat condensed on the fabric surface from flowing back to the skin.

We evaluate the effect of the twill fabric width on the sensitivity and explore the mechanism. The sensitivity is represented by the gauge factor (GF), which is calculated by $(\Delta R/R_0)/\epsilon$, where the ϵ is the strain of the sensor. Figure 3a exhibits that the sensitivity of the GMF can be adjusted by changing the sensor width. The GMF sensor with a width of 2 cm acquires better sensitivity throughout 100% tensile strain compared to the GMF sensors with widths of 0.5 cm and 1 cm (Table S1). We demonstrate a simple electrical model in Fig. 3b to show the mechanism. The adjacent rGO-CGY in the GMF sensor with a width of 2 cm possesses more contact points due to its larger width. It can be understood that the sensor with a higher width enables the generation of more separation points between two adjacent conductive threads considering their longer contact edges. The increase in separation points at the same-degree strain deformation is related to relative resistance changes. These contact points are completely separated during the stretching process, leading to a higher relative resistance increase in the sensor. Therefore, the wider GMF sensor has better sensitivity. The continuous conductive CGYs without elongation form a parallel circuit, forming a hybrid circuit in the stretched state [51, 52]. The initial resistance (R) of the wider sensor and the narrower sensor can be calculated with Eq. (1) and Eq. (2).

$$R = n \frac{R_C R_2 + 2aR_1 R_C + 2a^2 R_1 R_2}{R_C + aR_2} \tag{1}$$

$$R = n \frac{R_C R_2 + 2bR_1 R_C + 2b^2 R_1 R_2}{R_C + bR_2}, \tag{2}$$

where R_1 and R_2 are the resistance of the linear part and cured part of the yarns, respectively, and R_C refers to the contact resistance between two adjacent yarns. The a and b are the numbers of contact points of the sensors with wide and narrow widths, respectively ($a > b > 1$). Equation (1) and Eq. (2) can depict the overall resistance of the sensor in the initial state. The conductive CGY undergoes a separation before maximum deformation. With the increase in the tensile elongation of the sensor, the contact area between

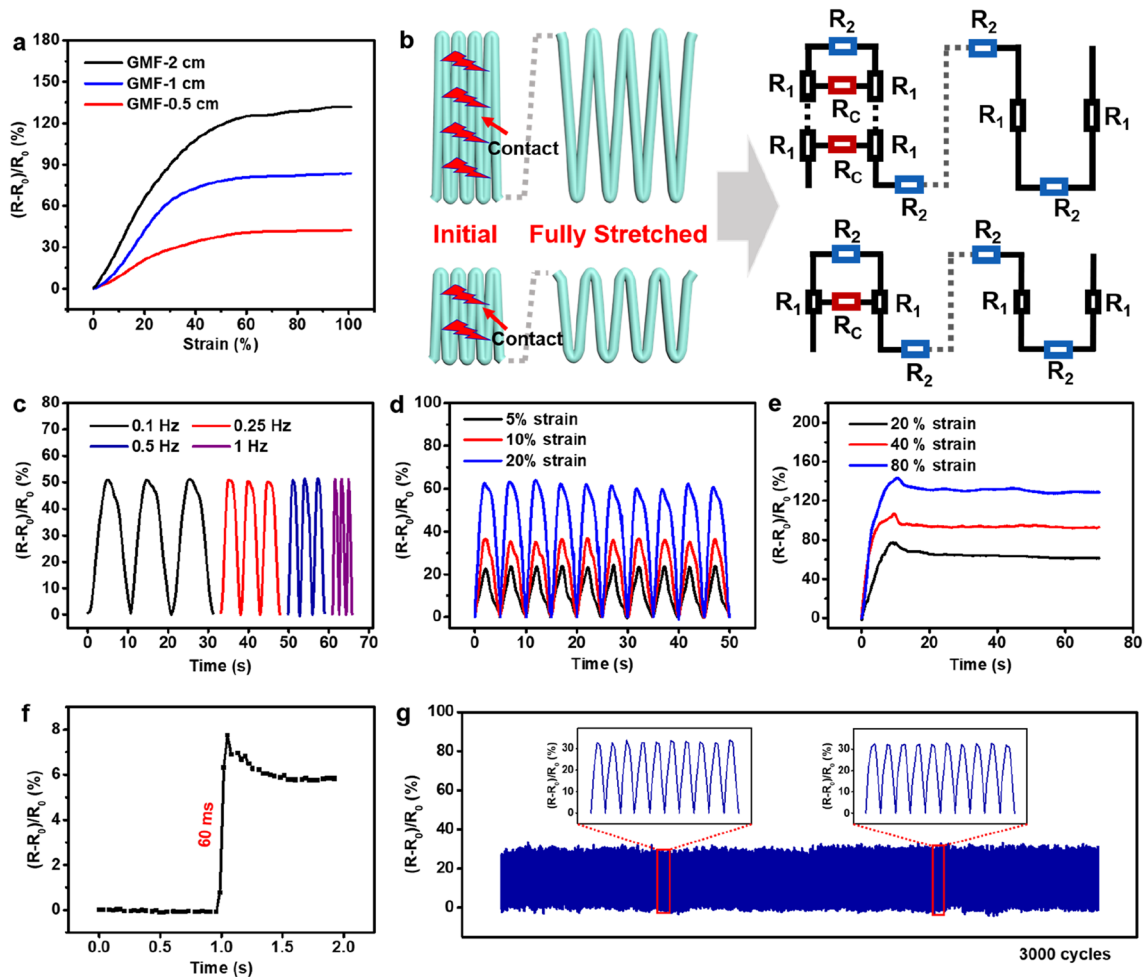


Fig. 3 Electrical responses of the GMF sensor and the corresponding mechanism. **a** The calibration of the GMF sensors with different widths. **b** Electrical model of the sensors, displaying their sensing mechanism. **c** Electrical response to stretching-releasing strain (15%) at various frequencies ranging from 0.1 to 1 Hz, showing the dynamic stability of the sensor. **d** Electrical response to stretching-releasing

strain (5–20%) at a frequency of 0.5 Hz, showing the dynamic stability of the sensor. **e** The relative resistance changes of the sensor with a step strain, exhibiting low creep and static stability. **f** The response time of the sensor subjected to a fast-speed 0.5% strain, which can reach ≈ 60 ms. **g** Cyclic durability of the sensor under a stretching-releasing strain of 10% for 3000 cycles with a frequency of 0.5 Hz

adjacent conductive yarns decreases, thus causing the contact resistance (R'_C) to increase. The R increases with the increase of R_C , which leads to an incremental resistance of the sensor. In this case, the resistance (R') of the sensor can be calculated according to Eq. (3). This explains the mechanism of the stretch-induced increasing resistance of the sensor.

$$R' = m \frac{R'_C R_2 + 2R_1 R'_C + 2R_1 R_2}{R'_C + R_2} + (n - m)(2R_1 + R_2) \quad (3)$$

In Fig. S8a, we compare the sensitivity of the GMF sensors with a width of 2 cm fabricated by the rGO-CGYs treated with 7 and 10 applications of the rGO coating, which implies that the volume conductivity of the crosswise yarn

is positively correlated with the sensitivity of the sensors. Fig. S8b presents that the GMF sensor (plain structure) with a width of 2 cm has lower sensitivity throughout the 100% strain deformation process compared with the abovementioned sensor with a twill structure. The difference is mainly attributed to the distinct contact areas between adjacent conductive yarns in the plain and twill structures. Compared with the sensor with a plain structure, the adjacent rGO-CGYs in the twill-structure sensor have a larger contact area, resulting in lower contact resistance (Figs. S8c–d). In the process of stretching and separating, the crosswise yarns experience more changes in the contact area, endowing the GMF sensor (twill structure) with better sensitivity.

Figure 3c illustrates the dynamic stability by applying a periodic stretching-releasing strain of 15% at frequencies ranging from 0.1 to 1 Hz. Similarly, we apply periodic

stretching-releasing strains of 5%, 10% and 20% with a frequency of 0.5 Hz to show the dynamic strain stability. The repeatable electrical outputs at each frequency and strain level confirm the dynamic stability of the GMF sensors. The stability is beneficial from the longitudinal elastic yarns in the fabric structure, ensuring the repeatable and stable separation and recovery of the conductive threads during loading-uploading strain (Fig. S9). When tensile strains of 20%, 40%, and 80% are applied to the sensor, the electrical signal in Fig. 3e exhibits slight overshoots and quickly becomes stable, illustrating the outstanding static stability of the GMF sensor. To precisely determine the response speed, a quasi-transient step strain of 0.5% with a speed of 16 mm/s was applied to the sensor. Figure 3f displays that the response time of the sensor (≈ 60 ms), which is adequate to meet the general needs of strain sensing applications. To further assess the stability and durability of the sensor, a loading-upload strain of 10% was applied to it at a frequency of 0.5 Hz for 3000 cycles. The electrical response in Fig. 3g is reproducible throughout the whole process with slight fluctuations, demonstrating the outstanding durability of the lossless sensing networks. We washed the GMF sensor with laundry liquid at room temperature (30 °C) for 45 min (Fig. S10a) and compared the electrical responses of the sensor after repeated washing. The sensitivity decreases moderately with increasing washing cycles (Fig. S10b), which profits from the strong hydrogen bonding between the CGY and the rGO [43]. It is worth noting that the sensitivity of the GMF sensor is similar to the unwashed sensor throughout the working range after 5 washing cycles.

Unlike conventional sensors that ignore unstable sensing performance caused by human body temperature and humidity changes, the GMF sensor shows high sensing stability towards wearable microclimate changes. As shown in Fig. 4a, a closed space was built and the environment was heated with a blower to evaluate the static and dynamic stability of the sensor during the heating process. Figure 4b displays the electrical response of the GMF sensor under a cyclic strain of 15% in changeable temperature. The signals keep stability with highly reproducible signaling patterns when the temperature increases from 22.8 to 47.3 °C. Additionally, the sensor illustrates excellent stability towards temperature changes in static conditions (Fig. 4c). The electrical conduction of the networked rGO thin film can be described by the hopping transport of carriers within and between the nanosheets. Carrier transport is expected to be greatly affected by the thermal effects of these carriers [53–56]. However, many negative groups existing in the GO, such as carboxyl and hydroxyl groups, are eliminated in the process of long-reduction time, which leads to smaller activated deep trap states (low-state density) and a short-range variable hopping of carriers between adjacent layers of the rGO (Fig. S11a). Therefore, the insensitivity of the GMF

sensor to temperature change is attributed to the rGO on the CGY surface exhibiting a decrease in the hopping charge transport number and the slight thermal generation of fewer carriers (Fig. S11b) [57]. The reduction in functional groups can also endow the sensor with a response that is insensitive to humidity simulations. We use a humidifier to adjust the humidity in the confined space to evaluate the sensor performance towards humidity changes (Fig. 4d). The sensor resistance in Fig. 4e remains stable at a relative humidity of $\approx 39\%$ and fluctuates moderately with increasing relative humidity up to $\approx 71\%$, which shows that the GMF sensor is insensitive to humidity changes. Similarly, the electrical signals of the sensor were measured under a recurrent strain of 15%, and the results indicate that the electrical response remains highly steady and repeatable during the humidity change process (Fig. 4f). The rGO endows the yarn with high hydrophobicity due to the oxygen-related functional groups on the CGY surface are eliminated, including hydroxyl and carboxyl groups, after reduction and water adsorption is minimized [47, 48], which enables the GMF sensor to stably output electrical signals regardless of humidity changes.

In monitoring human movement, friction inevitably arises between the sensor and the skin. To analyze the effect of wear-out issues on the electrical response of the GMF sensor, we tested the electrical signal of the sensor by applying a recurrent strain of 15% before and after applying friction to the sensor by hand. The electrical output of the sensor in Fig. 4g reveals that friction applied by hand would not impair the sensing ability and performance. Based on the abovementioned characterizations and demonstrations, the GMF sensors reveal conjunct assets, including fast response time, excellent durability, wide strain range, outstanding breathability, and reliability at various temperature and humidity values, that are superior to state-of-the-art strain sensors (Table S2).

Compared to traditional rubber-encapsulated strain sensors, the GMF sensor made from fibers can be nicely combined with clothing, which is imperative for practical wearing occasions. Figure 5a shows an image of a sensor sewn into cloth to illustrate that the sensor can be well integrated into clothes for sensing applications. We demonstrate a full-range body-sensing network by attaching sensors to different parts of the human body to monitor human motions (Fig. 5b). Slight epidermal movements caused by chewing, throat vibrations and respiration can be promptly and accurately captured by the GMF sensor. The electrical pattern obtained from gum chewing in Fig. 5c is reproducible, revealing the promise of its application prospects in oral locomotion and training. We attached the sensor to the throat to recognize the states of coughing and speaking. Figure 5d displays the resistance change of the sensor during coughing. There is an updown resistance change signal associated with the exertion and release of cough, respectively, which

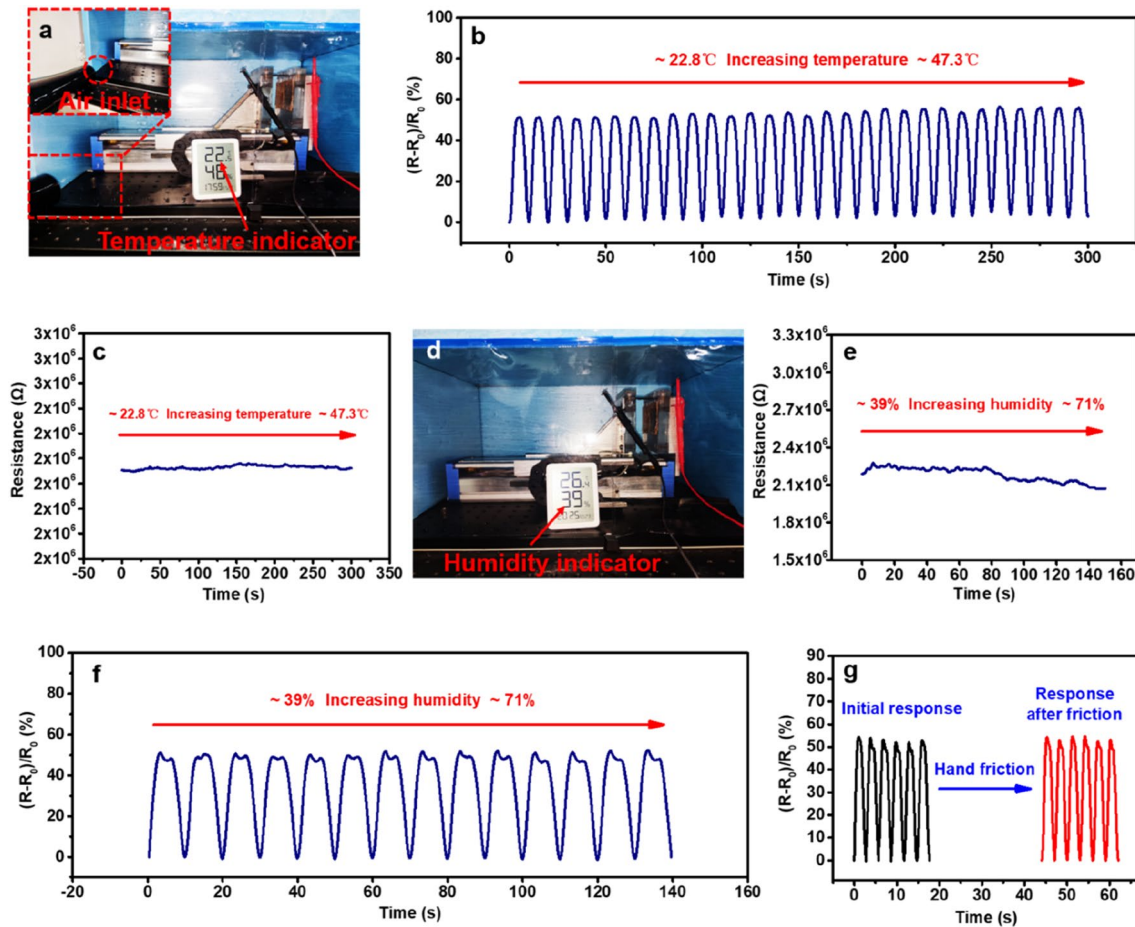


Fig. 4 The temperature and humidity dependence of the GMF sensor. **a** Image of the device constructed by the researchers to evaluate the influence of temperature change on the sensor. **b** Electrical signals of the sensor under a cyclic strain of 15% in the temperature from ≈ 22.8 °C (room temperature) to ≈ 47.3 °C, presenting stability of the sensor at different temperatures. **c** Relative resistance changes of the GMF sensor with the temperature rising from ≈ 22.8 to ≈ 47.3 °C.

d Image of the device constructed by the researchers to evaluate of the humidity dependence of the sensor. **e** Static stability of the sensor within a certain humidity range (from ≈ 39 to ≈ 71 %). **f** Electrical outputs of the GMF sensor with a recurrent strain of 15% in the process of humidity changing from ≈ 39 to ≈ 71 %, presenting stability of the sensor in different humidities. **g** Electrical signals of the GMF sensor before and after hand friction

is consistent with the expansion of corresponding epidermal vibrations. On the other hand, the electrical response is repeatable throughout with marginal deviations, indicating that the motion is tracked with a highly reproducible signaling pattern. In Fig. 5e, the resistance signals generated from speaking can be sensed by the sensor and exhibit differentiable and reproducible patterns when speaking various words (I love you, strain sensor and wearable). These signals of human normal breathing and breathing during running are collected in Fig. 5f, exhibiting a discernible respiratory rate and depth over the two diverse conditions.

The broad-sensing-range sensor can recognize not only tiny body movements but also detect large body deformations such as finger bending, walking and running, etc. We attached the sensor to the finger to monitor finger motion in Fig. 5f. It shows that the resistance fluctuates up and down

for bending the finger once, and the signals can be repeated and are highly consistent with the degree of finger bending. In addition, by applying the sensor to the skin surface of the wrist (Fig. 5h), the bending motion of the wrist can be detected. These electrical signals rise and fall with the wrist bending and straightening (Fig. 5h), which demonstrates the potential application in wrist bending-related sports, such as basketball, volleyball and skating, by appropriately embedding sensors in wristbands. Fig. S12 demonstrates nodding motion monitoring and reveals that the motion is explicitly reflected by the sensor. For further demonstrations of large limb movement detection, we measured the relative resistance changes of the sensor during walking and running. The measurement results indicate that the movements are accurately discriminated by the response frequency and intensity of the sensor, where the walking and running speeds are

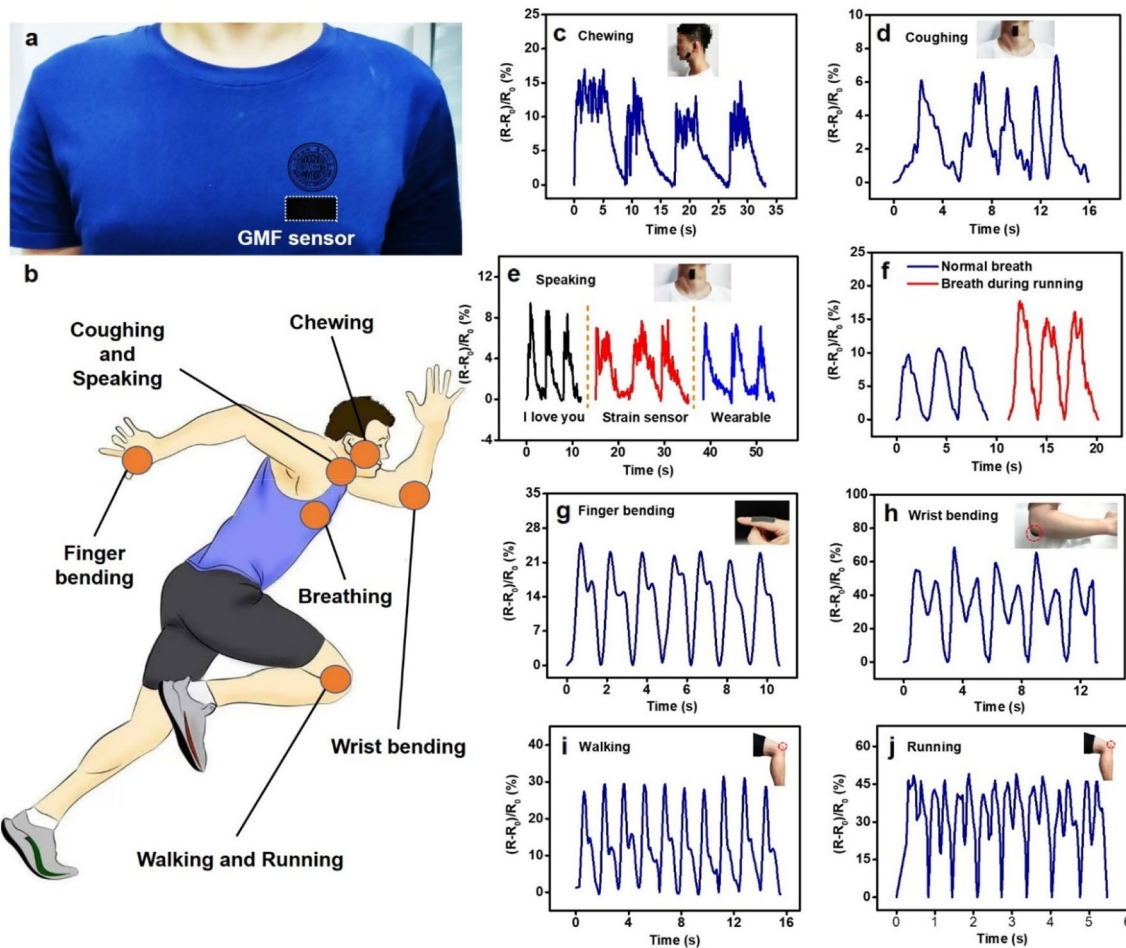


Fig. 5 Application demonstration of the GMF sensor. **a** Integration of the sensor with clothes, showing its good compatibility. **b** An overview of the location of the body-sensing network. **c** Corresponding signals of chewing gum. **d** Relative electrical resistance changes of throat vibration during coughing. **e** Signals of the throat epidermis

vibration while speaking different words. **f** Relative electrical resistance changes during normal breathing and breathing during running. **g** Signals of index finger bending from the sensor. **h** Electrical output during wrist bending. **i** The relative resistance changes during walking. **j** Electrical response during running

$\approx 1.6 \text{ s steps}^{-1}$ and $\approx 0.68 \text{ s steps}^{-1}$, respectively. The sensor retains high reliability and stability during walking and running and has great potential applications in sports training. Because of the high sensing stability, real-time recognition, wide sensing range, excellent breathability, and insensitivity to temperature and humidity changes, the sensor can be applied for monitoring subtle and violent physical deformation, which is of great significance for timely detection of human diseases and reconstruction through body-sensing networks.

Conclusions

In summary, a breathable strain sensor with tunable sensitivity is developed by constructing the rGO-CGY and elastic yarns into an independently crossed structure that exhibits

extremely low sensitivity to both temperature and humidity changes. Owing to the high-porosity of the fabric structure, the sensor displays excellent breathability to air and water vapor ($2.03 \text{ kg m}^{-2} \text{ h}^{-1}$). The GMF sensor shows attractive sensing performance, including a fast response speed ($< 60 \text{ ms}$) and high durability (> 3000 cycles), and tunable sensitivity by simply altering the width of the fabric. More importantly, taking advantage of the rGO with high hydrophobicity and insensitivity to temperature and humidity changes after a long-reduction time, the sensor possesses sensing independence against temperature and relative humidity in the ranges of $22.8\text{--}47.3 \text{ }^\circ\text{C}$ and $39\text{--}71\%$, respectively. In particular, the concept of using independent elastic and conductive yarns for the construction of strain sensors can be rapidly extended to various fabric-based wearable sensors, paving a new way for the low production cost and

scalable fabrication of highly breathable, high-performance, encapsulation-free, and reliable sensing strain sensors.

Supplementary Information The online version contains supplementary material available at <https://doi.org/10.1007/s42765-023-00270-y>.

Acknowledgements This work was financially supported by the National Key R&D Program of China (2021YFE0111100), Ministry of Science and Technology of the People's Republic of China (KY202201002), the Jiangsu Provincial Department of Science and Technology (BZ2022017) and the Shanghai Science and Technology Committee (21015800600). We would like to thank the China National Textile and Apparel Council (J202002), Jiangsu Advanced Textile Engineering Technology Center (XJFZ/2021/7) and projects with number 2021-fx010104 for their support.

Data availability Data available within the article or its supplementary materials.

Declarations

Conflict of Interest The authors declare that they have no known competing financial interests or personal relationships.

Open Access This article is licensed under a Creative Commons Attribution 4.0 International License, which permits use, sharing, adaptation, distribution and reproduction in any medium or format, as long as you give appropriate credit to the original author(s) and the source, provide a link to the Creative Commons licence, and indicate if changes were made. The images or other third party material in this article are included in the article's Creative Commons licence, unless indicated otherwise in a credit line to the material. If material is not included in the article's Creative Commons licence and your intended use is not permitted by statutory regulation or exceeds the permitted use, you will need to obtain permission directly from the copyright holder. To view a copy of this licence, visit <http://creativecommons.org/licenses/by/4.0/>.

References

- Pan S, Liu Z, Wang M, Jiang Y, Luo Y, Wan C, Qi D, Wang C, Ge X, Chen XJ. Mechanocombinatorially screening sensitivity of stretchable strain sensors. *Adv Mater*. **2019**;31:1903130.
- Zhai H, Xu L, Liu Z, Jin L, Yi Y, Zhang J, Fan Y, Cheng D, Li J, Liu XJ. Twisted graphene fibre based breathable, wetttable and washable anti-jamming strain sensor for underwater motion sensing. *Chem Eng J*. **2022**;439: 135502.
- Liu Z, Li Z, Yi Y, Li L, Zhai H, Lu Z, Jin L, Lu JR, Xie SQ, Zheng ZJ. Flexible strain sensing percolation networks towards complicated wearable microclimate and multi-direction mechanical inputs. *Nano Energy*. **2022**;99: 107444.
- Liu Z, Li Z, Zhai H, Jin L, Chen K, Yi Y, Gao Y, Xu L, Zheng Y, Yao SJ. A highly sensitive stretchable strain sensor based on multi-functionalized fabric for respiration monitoring and identification. *Chem Eng J*. **2021**;426: 130869.
- Gandla S, Naqi M, Lee MG, Lee JJ, Won Y, Pujar P, Kim J, Lee SH, Kim S. Highly linear and stable flexible temperature sensors based on laser-induced carbonization of polyimide substrates for personal mobile monitoring. *Adv Mater Technol*. **2020**;5:2000014.
- Wang YM, Zhang LW, Zhang ZW, Sun PY, Chen HW. High-sensitivity wearable and flexible humidity sensor based on graphene oxide/non-woven fabric for respiration monitoring. *Langmuir*. **2020**;36:9443–8.
- Yamada T, Hayamizu Y, Yamamoto Y, Yomogida Y, Izadi-Najafabadi A, Futaba DN, Hata K. A stretchable carbon nanotube strain sensor for human-motion detection. *Nat Nanotechnol*. **2011**;6:296–301.
- Pan J, Yang M, Luo L, Xu A, Tang B, Cheng D, Cai G, Wang X. Stretchable and highly sensitive braided composite yarn@polydopamine@ polypyrrole for wearable applications. *ACS Appl Mater Interfaces*. **2019**;11:7338–48.
- Yang Z, Pang Y, Han X-I, Yang Y, Ling J, Jian M, Zhang Y, Yang Y, Ren T-L. Graphene textile strain sensor with negative resistance variation for human motion detection. *ACS Nano*. **2018**;12:9134–41.
- Liu H, Li Q, Bu Y, Zhang N, Wang C, Pan C, Mi L, Guo Z, Liu C, Shen C. Stretchable conductive nonwoven fabrics with self-cleaning capability for tunable wearable strain sensor. *Nano Energy*. **2019**;66: 104143.
- Zhu C, Wu J, Yan J, Liu X. Advanced fiber materials for wearable electronics. *Adv Fiber Mater*. **2022**. <https://doi.org/10.1007/s42765-022-00212-0>.
- Sun L, Huang H, Ding Q, Guo Y, Sun W, Wu Z, Qin M, Guan Q, You Z. Highly transparent, stretchable, and self-healable ionogel for multifunctional sensors, triboelectric nanogenerator, and wearable fibrous electronics. *Adv Fiber Mater*. **2022**;4:98–107.
- Souri H, Bhattacharyya D. Highly stretchable multifunctional wearable devices based on conductive cotton and wool fabrics. *ACS Appl Mater Interfaces*. **2018**;10:20845–53.
- Sun S, Liu Y, Chang X, Jiang Y, Wang D, Tang C, He S, Wang M, Guo L, Gao Y. A wearable, waterproof, and highly sensitive strain sensor based on three-dimensional graphene/carbon black/Ni sponge for wirelessly monitoring human motions. *J Mater Chem C*. **2020**;8:2074–85.
- Liu Z, Zhu T, Wang J, Zheng Z, Li Y, Li J, Lai YJ. Functionalized fiber-based strain sensors: pathway to next-generation wearable electronics. *Nano-Micro Lett*. **2022**;14:1–39.
- Hu X, Huang T, Liu Z, Wang G, Chen D, Guo Q, Yang S, Jin Z, Lee J-M, Ding G. Conductive graphene-based E-textile for highly sensitive, breathable, and water-resistant multimodal gesture-distinguishable sensors. *J Mater Chem A*. **2020**;8:14778–87.
- Kim S-R, Lee S, Kim J, Kim E, Kil H-J, Yoo J-H, Oh J-H, Jeon J, Lee E-I, Jeon J-W. A fabric-based multifunctional sensor for the early detection of skin decubitus ulcers. *Biosens Bioelectron*. **2022**;215: 114555.
- Zhao Z, Huang Q, Yan C, Liu Y, Zeng X, Wei X, Hu Y, Zheng Z. Machine-washable and breathable pressure sensors based on triboelectric nanogenerators enabled by textile technologies. *Nano Energy*. **2020**;70: 104528.
- Luo J, Gao S, Luo H, Wang L, Huang X, Guo Z, Lai X, Lin L, Li RK, Gao JJ. Superhydrophobic and breathable smart MXene-based textile for multifunctional wearable sensing electronics. *Chem Eng J*. **2021**;406: 126898.
- Liu Z, Zheng Y, Jin L, Chen K, Zhai H, Huang Q, Chen Z, Yi Y, Umar M, Xu LJ. Highly breathable and stretchable strain sensors with insensitive response to pressure and bending. *Adv Funct Mater*. **2021**;31:2007622.
- Lu D, Liao S, Chu Y, Cai Y, Wei Q, Chen K, Wang Q. Highly durable and fast response fabric strain sensor for movement monitoring under extreme conditions. *Adv Fiber Mater*. **2022**. <https://doi.org/10.1007/s42765-022-00211-1>.
- Liu X, Miao J, Fan Q, Zhang W, Zuo X, Tian M, Zhu S, Zhang X, Qu L. Recent progress on smart fiber and textile based wearable strain sensors: materials, fabrications and applications. *Adv Fiber Mater*. **2022**;4:361–89.
- Li Q, Ding C, Yuan W, Xie R, Zhou X, Zhao Y, Yu M, Yang Z, Sun J, Tian Q. Highly stretchable and permeable conductors

- based on shrinkable electrospun fiber mats. *Adv Fiber Mater.* **2021**;3:302–11.
24. Wen D-L, Pang Y-X, Huang P, Wang Y-L, Zhang X-R, Deng H-T, Zhang X-S. Silk fibroin-based wearable all-fiber multifunctional sensor for smart clothing. *Adv Fiber Mater.* **2022**;4:873–84.
 25. Kang S, Zhao K, Yu D-G, Zheng X, Huang C. Advances in biosensing and environmental monitoring based on electrospun nanofibers. *Adv Fiber Mater.* **2022**;4:404–35.
 26. Tan C, Dong Z, Li Y, Zhao H, Huang X, Zhou Z, Jiang J-W, Long Y-Z, Jiang P, Zhang T-Y. A high performance wearable strain sensor with advanced thermal management for motion monitoring. *Nat Commun.* **2020**;11:1–10.
 27. Son D, Kang J, Vardoulis O, Kim Y, Matsuhisa N, Oh JY, To JW, Mun J, Katsumata T, Liu Y. An integrated self-healable electronic skin system fabricated via dynamic reconstruction of a nanostructured conducting network. *Nat Nanotechnol.* **2018**;13:1057–65.
 28. Zhang D, Zhang K, Wang Y, Wang Y, Yang YJ. Thermoelectric effect induced electricity in stretchable graphene-polymer nanocomposites for ultrasensitive self-powered strain sensor system. *Nano Energy.* **2019**;56:25–32.
 29. Gao Y, Li Q, Wu R, Sha J, Lu Y, Xuan FJ. Laser direct writing of ultrahigh sensitive SiC-based strain sensor arrays on elastomer toward electronic skins. *Adv Funct Mater.* **2019**;29:1806786.
 30. D'Souza RJ, Varun M, Masih J, Paul MS. Identification of *Calotropis procera* L. as a potential phytoaccumulator of heavy metals from contaminated soils in Urban North Central India. *J Hazard Mater.* **2010**;184:457–64.
 31. Zheng Y, Cao E, Zhu Y, Wang A, Hu H. Perfluorosilane treated *Calotropis gigantea* fiber: instant hydrophobic–oleophilic surface with efficient oil-absorbing performance. *Chem Eng J.* **2016**;295:477–83.
 32. Chen Q, Zhao T, Wang M, Wang J. Studies of the fibre structure and dyeing properties of *Calotropis gigantea*, kapok and cotton fibres. *Color Technol.* **2013**;129:448–53.
 33. Geim AK, Novoselov KS. The rise of graphene. *Nat Mater.* **2007**;6:183–91.
 34. Molina J. Graphene-based fabrics and their applications: a review. *RSC Adv.* **2016**;6:68261–91.
 35. Paulchamy B, Arthi G, Lignesh B. A simple approach to stepwise synthesis of graphene oxide nanomaterial. *Nanomater.* **2015**;6:1.
 36. Zhao ZY, Zheng ZZ, Chen P, Zhang HF, Yang CY, Wang XQ, Li G. Pre-treatment of *Calotropis gigantea* fibers with functional plasticizing and toughening auxiliary agents. *Text Res J.* **2019**;89:3997–4006.
 37. Ding XT, Bai J, Xu T, Li CX, Zhang HM, Qu LT. A novel nitrogen-doped graphene fiber microelectrode with ultrahigh sensitivity for the detection of dopamine. *Electrochem Commun.* **2016**;72:122–5.
 38. Sheng LZ, Wei T, Liang Y, Jiang LL, Qu LT, Fan ZJ. Ultra-high toughness all graphene fibers derived from synergetic effect of interconnected graphene ribbons and graphene sheets. *Carbon.* **2017**;120:17–22.
 39. Park SK, Seong CY, Piao Y. A simple dip-coating approach for preparation of three-dimensional multilayered graphene-metal oxides hybrid nanostructures as high performance lithium-ion battery electrodes. *Electrochim Acta.* **2015**;176:1182–90.
 40. Balandin AA, Ghosh S, Bao WZ, Calizo I, Teweldebrhan D, Miao F, Lau CN. Superior thermal conductivity of single-layer graphene. *Nano Lett.* **2008**;8:902–7.
 41. Dikin DA, Stankovich S, Zimney EJ, Piner RD, Dommett GHB, Evmenenko G, Nguyen ST, Ruoff RS. Preparation and characterization of graphene oxide paper. *Nature.* **2007**;448:457–60.
 42. Mackin TJ, Warren PD, Evans AG. Effects of fiber roughness on interface sliding in composites. *Acta Metall Mater.* **1992**;40:1251–7.
 43. Zhang J, Liu J, Zhao Z, Huang D, Chen C, Zheng Z, Fu C, Wang X, Ma Y, Li Y. A facile scalable conductive graphene-coated *Calotropis gigantea* yarn. *Cellulose.* **2022**;29:3545–56.
 44. Wang C, Zhang M, Xia K, Gong X, Wang H, Yin Z, Guan B, Zhang YJ. Intrinsically stretchable and conductive textile by a scalable process for elastic wearable electronics. *ACS Appl Mater Interfaces.* **2017**;9:13331–8.
 45. Xu LL, Guo MX, Liu S, Bian SW. Graphene/cotton composite fabrics as flexible electrode materials for electrochemical capacitors. *RSC Adv.* **2015**;5:25244–9.
 46. Cai GM, Xu ZL, Yang MY, Tang B, Wang XG. Functionalization of cotton fabrics through thermal reduction of graphene oxide. *Appl Surf Sci.* **2017**;393:441–8.
 47. Zhang GJ, Guo XX, Wang SL, Wang XL, Zhou YP, Xu H. New graphene fiber coating for volatile organic compounds analysis. *J Chromatogr B.* **2014**;969:128–31.
 48. Bhattacharjee S, Macintyre CR, Bahl P, Kumar U, Wen X, Aguey-Zinsou KF, Chughtai AA, Joshi R. Reduced graphene oxide and nanoparticles incorporated durable electroconductive silk fabrics. *Adv Mater Interfaces.* **2020**;7:2000814.
 49. Chen PY, Sodhi J, Qiu Y, Valentin TM, Steinberg RS, Wang ZY, Hurt RH, Wong IY. Multiscale graphene topographies programmed by sequential mechanical deformation. *Adv Mater.* **2016**;28:3564.
 50. Xu L, Liu Z, Zhai H, Chen X, Sun R, Lyu S, Fan Y, Yi Y, Chen Z, Jin LJ. Moisture-resilient graphene-dyed wool fabric for strain sensing. *ACS Appl Mater Interfaces.* **2020**;12:13265–74.
 51. Kim K-H, Hong SK, Ha S-H, Li L, Lee HW, Kim J-M. Enhancement of linearity range of stretchable ultrasensitive metal crack strain sensor via superaligned carbon nanotube-based strain engineering. *Mater Horiz.* **2020**;7:2662–72.
 52. Wang C, Li X, Gao E, Jian M, Xia K, Wang Q, Xu Z, Ren T, Zhang Y. Carbonized silk fabric for ultrastretchable, highly sensitive, and wearable strain sensors. *Adv Mater.* **2016**;28:6640–8.
 53. Eda G, Mattevi C, Yamaguchi H, Kim H, Chhowalla M. Insulator to semimetal transition in graphene oxide. *J Phys Chem C.* **2009**;113:15768–71.
 54. Kaiser AB, Gómez-Navarro C, Sundaram RS, Burghard M, Kern K. Electrical conduction mechanism in chemically derived graphene monolayers. *Nano Lett.* **2009**;9:1787–92.
 55. Mattevi C, Eda G, Agnoli S, Miller S, Mkhoyan KA, Celik O, Mastrogianni D, Granozzi G, Garfunkel E, Chhowalla M. Evolution of electrical, chemical, and structural properties of transparent and conducting chemically derived graphene thin films. *Adv Funct Mater.* **2009**;19:2577–83.
 56. Jung I, Dikin DA, Piner RD, Ruoff RS. Tunable electrical conductivity of individual graphene oxide sheets reduced at “low” temperatures. *Nano Lett.* **2008**;8:4283–7.
 57. Trung TQ, Le HS, Dang TML, Ju S, Park SY, Lee NE. Free-standing, fiber-based, wearable temperature sensor with tunable thermal index for healthcare monitoring. *Adv Healthcare Mater.* **2018**;7:1800074.



Junze Zhang is a Ph.D. student in the School of Fashion and Textiles, The Hong Kong Polytechnic University. He received Master degree in Textile Engineering from Soochow University of China in 2022. His research interests focus on nanomaterials and functionalized materials for the development of advanced composites, functional textiles, biomedical devices and flexible electronics.



Jing Liu is currently a Master student in National Engineering Laboratory for Modern Silk of Soochow University in China. Her research mainly focuses on silk-based flexible electronics, composite materials and wearable sensors.



Zeyu Zhao is a Ph.D. student in the Department of Applied Physics, The Hong Kong Polytechnic University. He received his Master of engineering degree in Textile Engineering from Soochow University of China in 2020. His research interests focus on organic electronics, chemical and biological sensors, wearable electronic devices and biomedical textiles.



Weiwei Sun is a Ph.D. student in the College of Textile and Clothing Engineering in Soochow University of China. He received his master's degree in materials and science engineering from

Beijing Institute of Graphic Communication in 2019. His current research mainly focuses on silk-based biomaterials and biosensors.



Gaojuan Zhao received his Ph.D. degree at Kunming Institute of Botany, Chinese Academy of Sciences. He has published over 30 academic articles and filed 2 patents. His research interests focus on tree species selection, breeding, ecological restoration and agroforestry system construction in hot-dry valley and karst ecologically fragile areas, especially for the cultivation and fiber development of woody fiber plants.



Jingge Liu is a senior undergraduate student of the College of Textile and Clothing Engineering in Soochow University. He has won top scholarship and spiritual civilization award several times. His research interests focus on fiber-based wearable sensors.



Jianchu Xu is a principal Scientist of the World Agroforestry Center, as well as a Distinguished Professor of the Kunming Institute of Botany, Chinese Academy of Sciences. He is famous expert in interdisciplinary research on agroforestry system and landscape restoration. He is the top 1% of global scientists for the most cited researchers in plant and animal sciences in during 2017 and

2022, respectively. He is editor in chief for the journal of Circular Agricultural System. He is a coordinator of the Mountain Futures Program, which is a global initiative to support knowledge innovations for smallholders in mountain regions worldwide.



Yuling Li is a full professor at the Department of Textile Design and Industrial Economy at the Donghua University of China. He is a member of Expert Committee of China Cotton Textile Industry Association and a member of National Professional Standardization Techniques Commission. He has filed 50 issued patents. He has won Second Prizes for National Science and Technology Progress two times, and the First Prizes for China National Textile and Apparel Council of Science and

Technology Progress for six times. His research interests include ecological textile technology, fabric design, textile protective materials, textile composites and biomedical textile materials.



Zekun Liu received his Ph.D. degree at Department of Materials, The University of Manchester, United Kingdom. He is now working as a Research Associate at Nuffield Department of Orthopaedics, Rheumatology and Musculoskeletal Sciences, University of Oxford. His research interests include nanomaterials and functionalized materials for the development of advanced composites, functional textiles, biomedical devices and flexible electronics.



Yi Li is a full professor and chair in Textile Science and Engineering in the University of Manchester. He is a Life-Fellow of Royal Society of Art and International Biographical Association and Fellow of the Textile Institute. He is the Chairman of Textile Bioengineering and Informatics Society, deputy council chairman of International Digital Health and Intelligent Materials Innovation Alliance, and board chair of Fashion Big Data Foundation. His research focuses advancement of

emerging cross-disciplinary science and engineering of how to design and engineer biomaterials, drug delivery systems, medical devices, smart e-textiles, intelligent wearables for human psychological and physiological needs.



Gang Li is a full professor at the National Engineering Laboratory for Modern Silk, Soochow University of China. He is the 15th high level talent of “Top six talent peaks” in Jiangsu province of China. He received MEng. from Donghua University of China, and obtained his Ph.D. in Biomedical textiles and Engineering from the Hong Kong Polytechnic University. He is also a visiting professor of Tufts University in USA (Prof. David Kaplan’s team). He published over 100 academic articles and

issued 40 patents between 2006 and 2023. His research interests focus on biomedical materials, functional and smart textiles by combining silk-based materials, biomedical materials and textile engineering.